PERFORMANCE OF *SPI* POINT-SOURCE DATA ANALYSIS

Pierre Dubath[1], I. Kreykenbohm[2,1], J. Knödlseder[3], P. Connell[4], G. K. Skinner[3], A. Strong[5], P. Sizun[6], D. Attié[6], S. Schanne[6], B. Cordier[6], L. Bouchet[3], A. von Kienlin[5]

[1]*INTEGRAL* Science Data Center, Ch. d'Écogia 16, CH-1290 Versoix, Switzerland

[2]IAAT – Astronomie, Sand 1, D-72076 Tübingen, Germany

[3]CESR, 9, avenue du Colonel Roche, B.P. 4346, F-31028 Toulouse Cedex 4, France

[4]GACE - ICMUV, University of Valencia, Apdo 22085, E-46071 Valencia, Spain

[5]MPE, Giessenbachstr. 1, D-85748 Garching, Germany

[6]CEA Saclay, DSM/DAPNIA/Service d'Astrophysique, F-91191 Gif-sur-Yvette, France

ABSTRACT

Performances of *SPI* data analyses of point sources are assessed using the Crab observations gathered during the first year of *INTEGRAL* operations. At low and intermediate signal-to-noise (S/N) ratios, the errors for both positions and fluxes provided by the imaging reconstruction program *spiros* are perfectly consistent with the distributions of the results of independent analyses. For higher S/N, *spiros* underestimates the real uncertainties, certainly because it does not take into account systematic errors, which can become comparable, or even larger, than statistical ones. Realistic source confusion tests are carried out by adding simulated data to the Crab observation. These tests demonstrate that spurious results can be obtained when the source separation is equal or smaller than 2 degrees. However, reliable flux values can be obtained for closer sources if their positions are fixed in the data deconvolution process.

1. INTRODUCTION

The distributions of the results obtained for independent subsets of the Crab *SPI* observations are used to assess different types of point-source analysis errors. The ISDC science analysis pipeline is used, including in particular, the programs *spi_obs_hist* and *spi_obs_back* (Knödlseder 2004) for event binning and background modeling, and *spiros* (Skinner & Connell 2003) for image reconstruction. In all analyses a background proportional to the saturated Germanium events is assumed, and one scaling coefficient per detector is derived by *spiros* through the image reconstruction process (*spiros* background option 2) [1]. The Chi-squared optimization statistic is used in *spiros.*

[1]Except in single pointing analysis where only one scaling coefficient is derived for all detectors and pointings, (*spiros* background option 3)

Table 1. Number and size of Crab pointing groups

Number of pointings per group	Number of groups
1	264
5	52
10	26
15	17
20	13

2. POINTINGS GROUPS OF DIFFERENT SIZES

An energy band of 28 to 48 keV is first selected to test the high signal-to-background case (with *spiros* Crab detection significance always larger than 70 even in the single pointing cases). The *SPI* data from the Crab observations of revolutions 43, 44, 45 and 102 are divided into independent groups of N pointings. The 5 cases shown in Table 1 are considered.

For each of the 5 cases, the different groups are analyzed separately and the distributions of the resulting Crab positions and fluxes provide a measure of the errors. For example, a distribution of 17 results is obtained for the N=15 case. Figure 1 shows the Crab positions obtained in independent analyses of groups of single, 5, 10 and 20 pointings in four different panels.

For each group size, a Gaussian is fitted to the distribution of Crab positions and fluxes. Examples of distributions obtained with groups of N=10 are shown in Fig. 2.

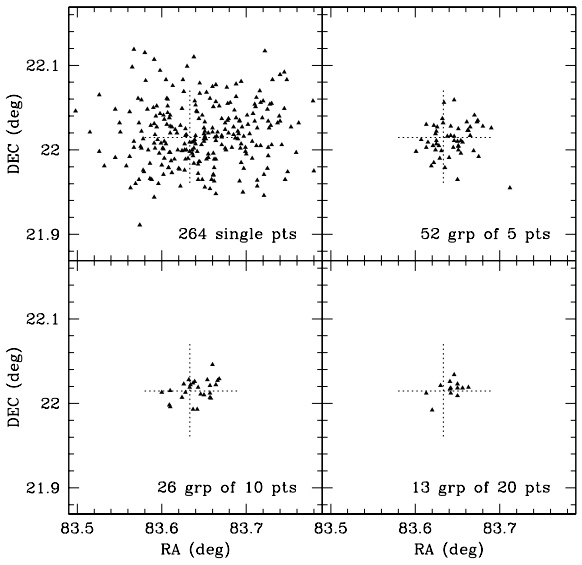

Figure 1. Each triangle in the four panels shows the Crab location resulting from one analysis of a group of either N = 1, 5, 10, or 20 pointings. The large dotted-line cross marks the catalogue Crab position (83.6332 - 22.0145 degree).

Means and standard deviations resulting from the Gaussian fits are also displayed in each panel. These distributions provide a measure of both systematic and statistical errors (except for the systematic on the Crab flux). Figure 2 shows that there may be some residual systematic error in RA at the level of 0.4 arcmin, despite the use of a misalignment matrix calibrated from the Crab and Cygnus X-1 data. Note however that 0.4 arcmin is only 0.3% of the FWHM of the response.

The standard deviations of all distributions are displayed as triangles - with small number statistic error bars - as a function of N, the group pointing number, in Fig. 3. The means of the errors provided directly by *spiros* represented as large dots underestimate the true errors certainly because of the importance of systematic errors in this case of high signal-to-background ratio. The *spiros* errors follow a $1/\sqrt{N}$-type of law, while the triangles are as consistent with such a law as with a straight line. This plot shows that systematic errors on position and flux are of the order of 0.5 arcmin and of 1%, respectively.

3. POINTING GROUPS WITH POSITION OFFSETS

The locations on the plane of the sky of all 264 pointings of our complete dataset are displayed as triangles in Fig. 4 (with the open circle showing the Crab position). In order to test for systematic effects with large offset angles, pointings are divided into groups following the dashed dividing lines. These 20 groups contain from 6 to 23 pointings, with an average of 13 pointings per group. Fig. 5 displays the distributions of the results derived from these

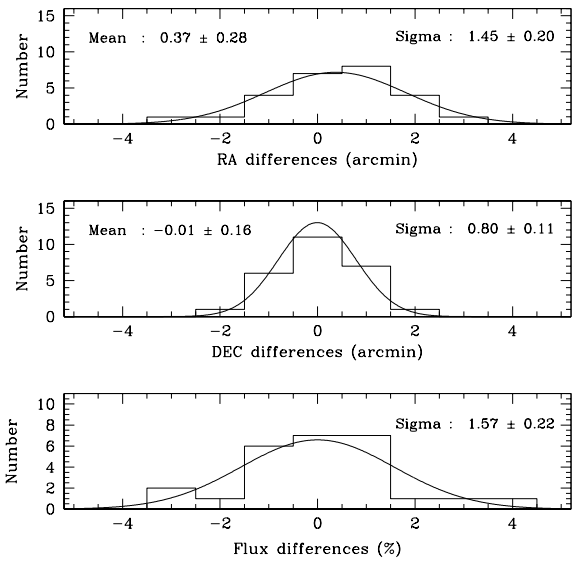

Figure 2. Distributions of the positions and fluxes obtained from analyses of 26 independent groups of 10 pointings. Positions are relative to the Crab catalogue position, while fluxes are relative to the mean flux. Means and standard deviations resulting from the Gaussian fits are displayed in each panel (except for the mean flux which is null by definition).

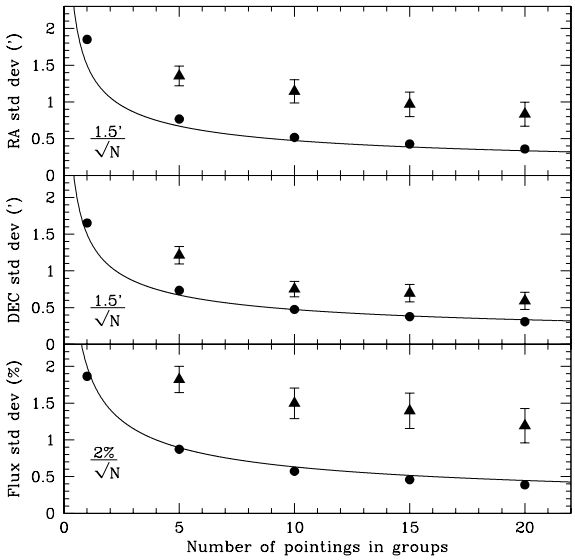

Figure 3. The standard deviations of all position and flux distributions – triangles with statistical error bars – are shown as a function of the group pointing number. The means of the errors provided directly by spiros are represented as large dots. They underestimate the true errors certainly because of the importance of systematic errors in this case of high signal-to-background ratio.

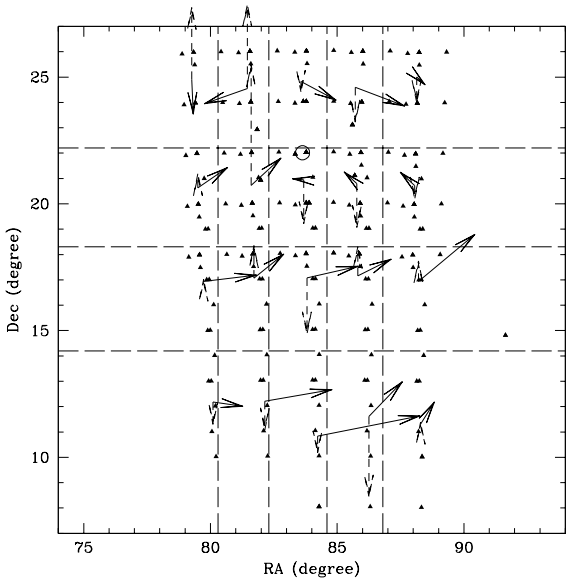

Figure 4. Triangles represent the locations of the 264 pointings of the Crab observations used in this study. These pointings are split into groups according to the boxes defined by the dashed lines. Arrows provide an illustration of the position (solid line) and flux (dashed line) errors resulting from the analysis of the corresponding pointing group (see text).

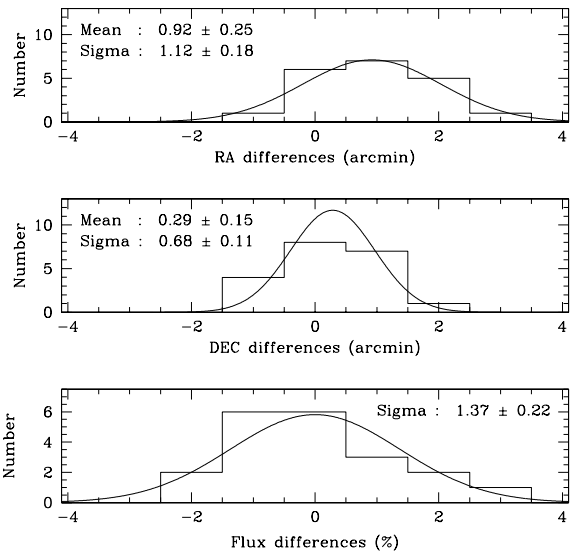

Figure 5. Distributions of the Crab position and flux results derived from the analysis of the 20 pointing groups defined by the dashed, dividing lines shown in Fig. 4. Positions are relative to the Crab catalogue position, while fluxes are relative to the mean flux. Means and standard deviations resulting from the Gaussian fits are displayed in each panel (except for the mean flux which is null by definition).

20 groups. The means and standard deviations are consistent with those of Fig. 2 showing that there is no obvious degradation with increasing offset angles. The systematic error in RA is more significant, but it remains relatively small (< 1'). Fig. 4 also shows the position (solid-line arrows) and flux (dashed-line arrow) error vectors arbitrarily scaled and shifted to appear on top of their respective group locations. These error vectors are computed as the difference between the positions resulting from the analyses and the catalogue position, and for the flux, as the difference to the mean value. Again, no obvious systematic error is observed in this figure.

4. ANALYSES WITH INCREASING NOISE LEVELS

Using the 17 groups of 15 consecutive pointings, analyses in narrower and higher energy bands are carried out to explore cases of decreasing signal-to-noise ratios. All results are obtained at relatively low energy (< 300 keV) where the instrument response does not change much with energy. In each case, a Gaussian function is fitted to the resulting RA, DEC, and flux distributions. The standard deviations and their statistical error bars are shown as a function of the mean detection significance given by *spiros* in Fig. 6. Our results are consistent with the mean errors provided by *spiros* displayed as open circles. The errors are consistent with a 90'/significance law. Note that the errors are here dominated by the statistical uncertainties as they are markedly larger than those of the high signal-to-background case shown in Fig. 3.

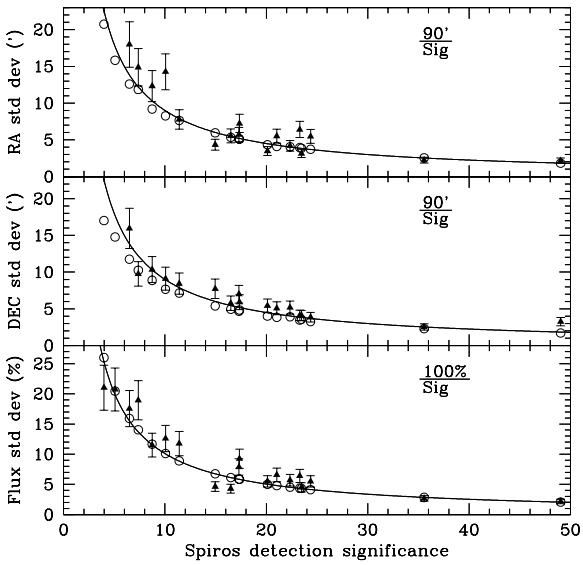

Figure 6. The standard deviations of all position and flux distributions – triangles with statistical error bars – are shown as a function of the spiros detection significance. The means of the errors provided directly by spiros are represented as large dots.

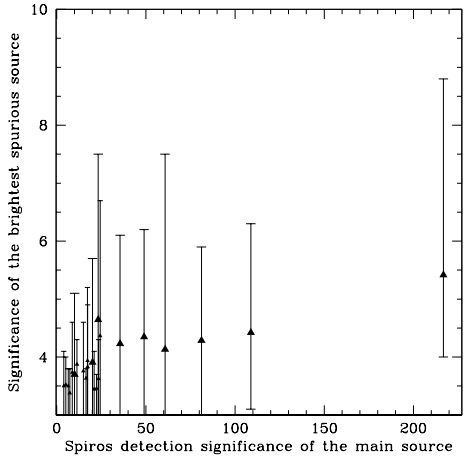

Figure 7. Significance of the second (spurious) source detected by spiros as a function of the detection significance of the main source. Error bars do not represent the usual standard deviation (displayed in all other plots), but the total range from the smallest to the largest obtained values.

Fig. 7 displays the significance of the second source detected by *spiros* as a function of the detection significance of the main source i.e. the Crab. The error bars in this case show the total range of the results, from the smallest to the largest values. These second sources are obviously not real as they appear at random positions in the plane of the sky. This figure shows that fake sources with significance up to 7 - 8 can be seen with *spiros* when a bright source is present in the field of view. The correlation with the significance of the main source is weak, although fake sources with significance larger than 5 are not seen when the main source has a significance smaller than $\sim$20.

5. SOURCE CONFUSION TESTS

In order to investigate the expected result degradations when sources are increasingly close to one another, an additional source is simulated and added to the Crab observation. In this approach, the simulated part is kept to a minimum as the background and one of the two sources come from an actual observation. The detector counts expected for a source close to the Crab location are computed for all 264 pointings of our dataset using the program *spi_add_sim* and the *SPI* instrumental response. 36 cases are considered with different separation angles (0.5, 1.0, 1.5, 2.0, 3.0 and 4.0 degree) and different flux ratios (1, 0.8, 0.6, 0.4, 0.3, and 0.2 of the Crab flux). An energy band 110-116 keV is selected. In this band, the *spiros* Crab detection significance is about 46 with 15 pointings, corresponding possibly to a more typical signal-to-background case. The computed counts are then added to the Crab data, and in each of the 36 cases, 17 analyses are carried out for independent groups of 15 pointings. Results are displayed in Fig. 8 and Fig. 9.

Different zones can be identified in Fig. 8. In the lower panels, the two sources are properly detected as

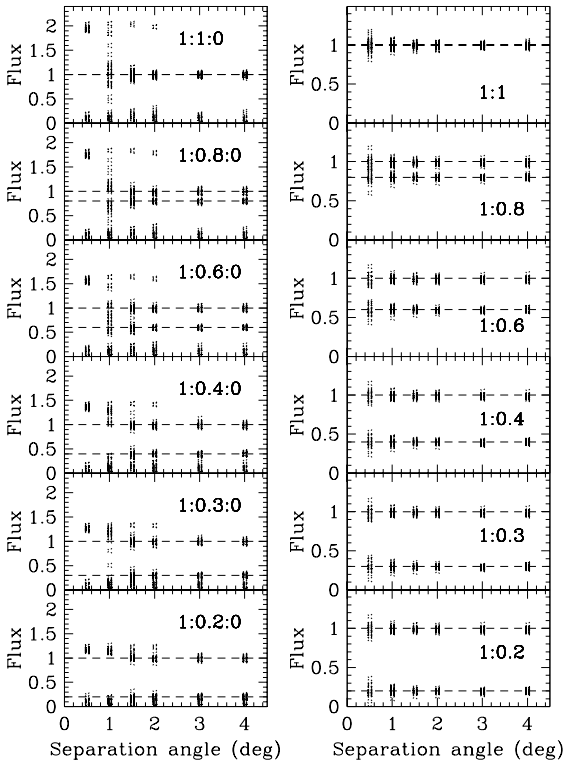

Figure 9. Left: Relative fluxes extracted by spiros at the positions displayed in Fig. 8, and right: relative fluxes extracted at the fixed known positions.

they should. In some cases of 2 deg separation angle, *spiros* starts to find only one "spurious" source instead of the two "real ones". The number of such cases increases with decreasing angle, and with 0.5 deg *spiros* detects only one source in all cases. Also note that the spurious source position is half way between the two actual sources when they have equal flux, and that this location moves towards the main real source position when the second source becomes weaker.

The left panels of Fig. 9, show that when *spiros* finds only one source, the resulting flux value is the sum of the Crab and of the simulated source values. Comparing the two columns of Fig. 9 points out the dramatic improvements obtained when fixing source positions in the flux extraction process.

REFERENCES

Knödlseder, J., 2004, these procedings

Skinner, G. & Connell, P. 2003, A&A, 411, L123

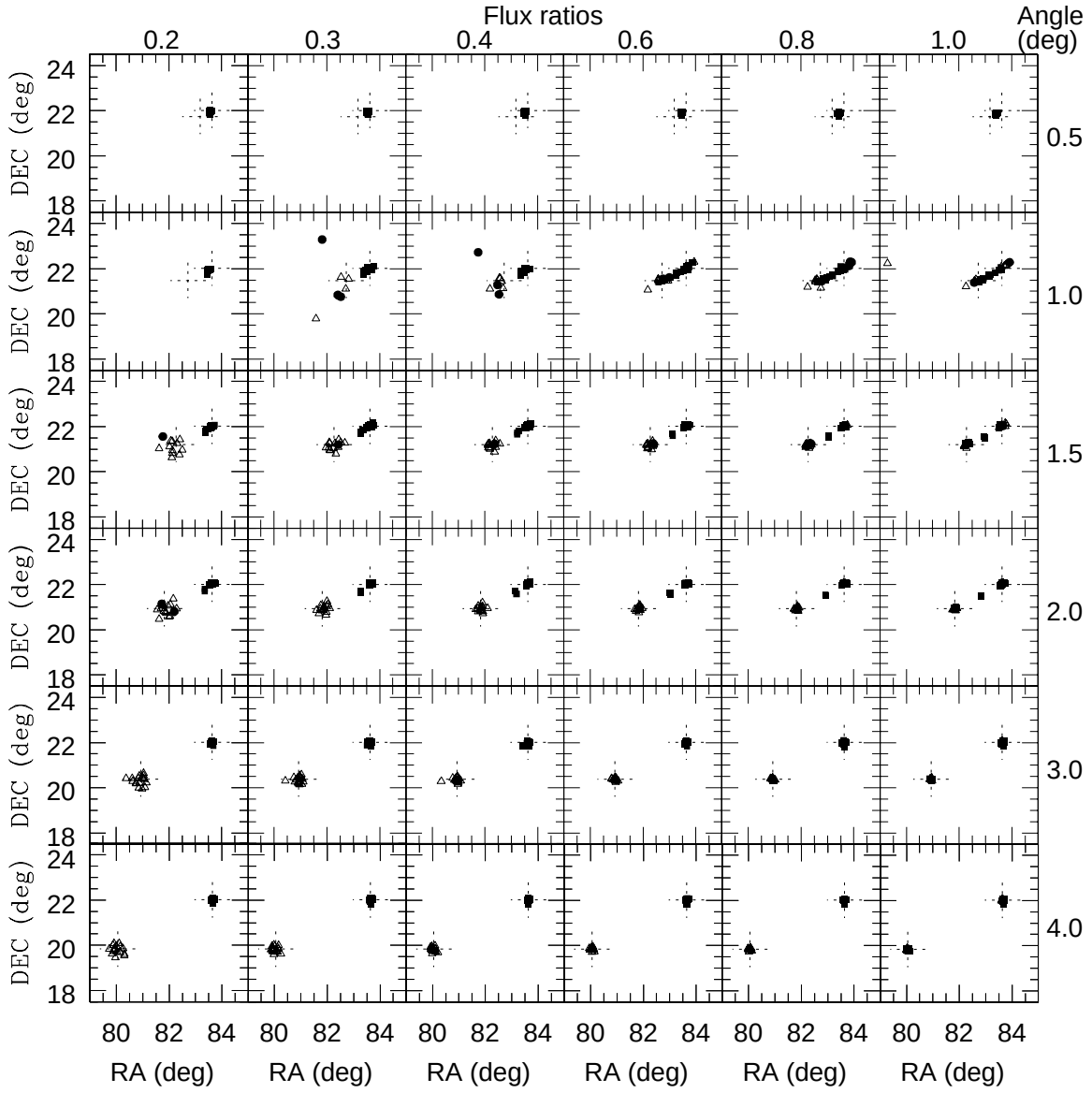

Figure 8. Locations of the first 3 brightest sources (above a threshold of 3 sigma) found by spiros in the analyses of different datasets, obtained by adding the contributions of a simulated source to the actual Crab INTEGRAL observation. The separation angles and flux ratios for the 36 studied cases are indicated around the main frame. Two large crosses show the input positions of the two real sources. In the lower panels, the two sources are properly detected as they should. In some cases of 2 deg separation angle, spiros starts to find only one "spurious" source instead of the two "real ones". The number of such cases increases with decreasing angle, and with 0.5 deg spiros detects only one source in all cases. Also note that the spurious source position is half way between the two actual sources when they have equal flux, and that this location moves towards the main real source position when the second source becomes weaker.